



HAL
open science

Discrete Ordinates and Monte Carlo Methods for Radiative Transfer Simulation Applied to Computational Fluid Dynamics Combustion Modeling

David Joseph, Patrice Perez, Mouna El-Hafi, Benedicte Cuenot

► **To cite this version:**

David Joseph, Patrice Perez, Mouna El-Hafi, Benedicte Cuenot. Discrete Ordinates and Monte Carlo Methods for Radiative Transfer Simulation Applied to Computational Fluid Dynamics Combustion Modeling. *Journal of Heat Transfer*, 2009, 131 (5), 10.1115/1.3013832 . hal-01712151

HAL Id: hal-01712151

<https://hal.science/hal-01712151>

Submitted on 8 Nov 2019

HAL is a multi-disciplinary open access archive for the deposit and dissemination of scientific research documents, whether they are published or not. The documents may come from teaching and research institutions in France or abroad, or from public or private research centers.

L'archive ouverte pluridisciplinaire **HAL**, est destinée au dépôt et à la diffusion de documents scientifiques de niveau recherche, publiés ou non, émanant des établissements d'enseignement et de recherche français ou étrangers, des laboratoires publics ou privés.

David Joseph
Patrice Perez

Centre de Recherche d'Albi en génie des
Procédés des Solides Divisés,
de l'Energie et de l'Environnement,
81000 Albi, France;
HPC-SA, 3 Chemin du Pigeonnier de la Cépière,
31100 Toulouse, France

Mouna El Hafi

Centre de Recherche d'Albi en génie des
Procédés des Solides Divisés,
de l'Energie et de l'Environnement,
81013 Albi, France
e-mail: elhafi@enstimac.fr

Bénédicte Cuenot

CERFACS,
42 Avenue Gaspard Coriolis,
31057 Toulouse, France

Discrete Ordinates and Monte Carlo Methods for Radiative Transfer Simulation Applied to Computational Fluid Dynamics Combustion Modeling

Modeling radiative heat transfer in combustion applications involving complex geometries and detailed spectral properties of radiative gaseous species remains a difficult challenge, especially when full coupling with detailed chemistry and fluid dynamics is required. The Monte Carlo method (MCM) usually considered as a reference "exact" method for the computation of radiative transfer is however very demanding in CPU-time. An alternative is the discrete ordinates method (DOM), based on a finite volume approach, that is more suitable for a direct coupling with computational fluid dynamics but may lack accuracy. The aim of the present paper is to propose and demonstrate the efficiency of a methodology for radiative transfer calculation, combining the advantages of both MCM and DOM. In this approach, the fast DOM is used to compute the radiative solution, and its accuracy is controlled by comparison with the exact MCM solution at a selected controlling points. A first application of the proposed methodology to an industrial burner prototype shows its validity and potential for the direct coupling of radiation calculations with unsteady reacting flow computations.

Keywords: radiative heat transfer, unsteady combustion, Monte Carlo, discrete ordinates, three-dimensional geometries

1 Introduction

Combustion simulation involves the treatment of coupled phenomena such as detailed chemistry, fluid mechanics and heat transfer for three-dimensional systems in complex geometries. The accurate treatment of thermal radiation is crucial if the aim is to predict the concentration of minor species, soot or wall heat fluxes that are highly dependent on temperature levels. However, the detailed calculation of radiative transfer leads to prohibitive computing time. This is even more critical for unsteady combustion simulations, where the full coupling with radiation is required.

The optically thin assumption is commonly used for the calculation of radiation in combustion simulations. In this approximation, the absorption of the gas mixture is neglected and only the emitted part of the radiative flux is considered, which considerably simplifies the calculation. This assumption may be justified in small scale non-sooty flames, although it may introduce significant errors in the prediction of pollutants [1]. In larger scale flames such as fire pools or furnaces, radiative absorption must be represented with good accuracy to predict radiative heat fluxes. In smaller industrial burners, it is known that the NO_x emission and soot production are very sensitive to radiation [2,3]. Wall heat fluxes are also critical parameters in burner design and should include radiative heat transfer [4].

In a recent work, Jensen et al. [5] compared the usual numerical methods for solving the radiative transfer equation (RTE). The ray tracing and Monte Carlo methods (MCMs) [6–9] allow to calculate quasixact solutions and are considered as reference methods.

In addition, MCM also provides estimates of the errors associated to the solution. It is able to treat high levels of complexity (complex geometries, reflective walls, scattering medium, gas spectral properties, etc.) and there is no conceptual difficulties to realize the coupling with flow dynamics. However these methods are complex and result in very high CPU costs. Many interesting ideas are actually under progress to reduce the computation time. Among them, the sensitivity approach (using first order of Taylor expansion) has been already tested in several applications [10,11] and showed good potential. Despite these improvements, the direct coupling of MCM with flow simulations is still not possible. On the contrary, the moment method [12], discrete ordinates method (DOM) [13,14], and the discrete transfer method [15] are fast and easy to couple with fluid dynamics, but they give approximate solutions. In particular the DOM is highly sensitive to the angular (ray effect) and spatial discretization. In Ref. [5], it is shown however that the DOM using the S_4 quadrature (24 discrete directions) already offers a very good compromise between CPU-time and accuracy and that the use of a higher order quadrature, such as the LC_{11} (96 discrete directions), provides accuracy levels comparable to the quasixact methods (MCM and ray tracing).

It is possible to take advantage of the availability of the two classes of methods by combining them in a global methodology, allowing fast radiation calculations with a systematic estimation and control of the error. The simultaneous use of the pair DOM (for the radiation computation)/MCM (for the a posteriori error control) is then an optimal compromise between CPU cost and accuracy in view of coupled combustion-radiation simulations. The benefit of this approach is double: First, it allows to validate the DOM solution, and second it determines the level of accuracy of the various approximations in order to optimize the set of parameters (number of directions, discretization scheme, etc.). The objective of the present paper is to describe the proposed approach

and demonstrate its validity and potential for future coupled radiation-combustion simulations on different test cases.

Compared with most existing radiation codes, the coupling of radiation with combustion requires additional developments. First, the complexity of real industrial geometries requires the use of unstructured grids. For an efficient coupling, the radiative transfer model should be able to work on the same mesh as the combustion simulation and therefore handle unstructured meshes. Second, the description of the gaseous radiative properties has to be in accordance with the combustion simulations accuracy. In this context, two radiative transfer codes, DOMASIU (based on DOM) and MCRAD (based on MCM), have been developed and applied to an unsteady combustion application following the above methodology.

In Sec. 2, the DOM and the MCM are briefly described. In Sec. 3, the DOM code, specifically developed for unstructured meshes, is validated against MCM on a nonisothermal and nonhomogeneous test case in a cylindrical geometry. Section 3.2 is devoted to the computation of thermal radiation in a real combustion chamber involving a complex geometry with an unstructured grid, using the combination of both DOM and MCM as explained above.

2 Mathematical Formulation

The two radiation codes DOMASIU and MCRAD used in the present study were initially developed by Joseph [1] and Perez [16]. DOMASIU is detailed in Ref. [14]. MCRAD has been utilized for benchmark publications and is described in Refs. [7] and [8]. The two codes have also been used in a pool fire problem where they have been compared with a ray tracing method, a discrete transfer method and a moment method [5], showing a good agreement with the reference solutions.

In all calculations presented in this paper, the same gas radiation property model (the statistical narrowband correlated- K model [17,18]) has been used. It is also described below.

2.1 Discrete Ordinates Method (DOM). DOMASIU [5,14] has been designed to simulate the radiative heat transfer in coupled simulations with flow dynamics, involving unstructured grids. In the following and for the sake of clarity, the intensities and radiative properties are expressed for a single wave number (monochromatic case), but the formulation can be easily extended to a full spectrum.

The discrete ordinates method has been introduced first by Chandrashekar [19] and have been widely used in radiative transfer applications. Considering an absorbing-emitting and non-scattering gray medium, the variation in the radiative intensity $I(\mathbf{s})$ along a line of sight can be written as

$$\frac{dI(\mathbf{s})}{ds} = \kappa I_b - \kappa I(\mathbf{s}) \quad (1)$$

where $I(\mathbf{s})$ is the radiative intensity along the directional coordinate \mathbf{s} , I_b is the blackbody radiative intensity, and κ is the absorption coefficient. Boundary conditions for diffuse surfaces are taken from the relation giving the intensity leaving the wall I_w as a function of the blackbody intensity of the wall $I_{b,w}$ and of the incident radiative intensity.

$$I_w(\mathbf{s}) = \epsilon_w I_{b,w} + \frac{\rho_w}{\pi} \int_{\mathbf{n} \cdot \mathbf{s}' < 0} I_w(\mathbf{s}') |\mathbf{n} \cdot \mathbf{s}'| d\Omega' \quad (2)$$

where ϵ_w is the wall emissivity, ρ_w is the wall reflectivity, \mathbf{n} is the unit vector normal to the wall, and \mathbf{s}' is the direction of propagation of the incident radiation confined within a solid angle $d\Omega'$.

2.1.1 Angular Discretization. In the DOM, the calculation of a radiative source term at a given point is based on the discretization of the radiative transfer equation (Eq. (1)) according to a chosen number N_{dir} of discrete directions $\mathbf{s}_i(\mu_i, \eta_i, \xi_i)$, associated with the corresponding weights w_i , contained in the solid angle

4π , and where (μ_i, η_i, ξ_i) are directional cosines. Different angular discretizations may be used. In a recent study, Koch and Becker [20] compared the efficiency of several types of angular quadratures. They recommend the LC₁₁ quadrature for its better accuracy. However calculations performed with the S_4 quadrature satisfy a good compromise between accuracy and rapidity as shown in Ref. [5], and may also be used.

2.1.2 Spatial Discretization for Hybrid Grids. The RTE (Eq. (1)) is solved for every discrete direction \mathbf{s}_i using a finite volume approach. The integration of the RTE over the volume V of an element limited by a surface Σ , and the application of the divergence theorem yields

$$\int_{\Sigma} I(\mathbf{s}_i) \cdot \mathbf{s}_i \cdot \mathbf{n} d\Sigma = \int_V (\kappa I_b - \kappa I(\mathbf{s}_i)) dV \quad (3)$$

The domain is discretized in three-dimensional control volumes V . It is assumed that I_b and $I(\mathbf{s}_i)$ are constants over the volume V and that the intensities I_j at the faces are constant over each face. Considering that I_j is the averaged intensity over the j th face, associated with the center of the corresponding face, that $I_{b,P}$ and I_P are the averaged intensities over the volume V , associated with the center of the cell, and assuming plane faces and vertices linked by straight lines, Eq. (3) can be discretized as follows:

$$\sum_{j=1}^{N_{face}} I_j(\mathbf{s}_i) \cdot (\mathbf{s}_i \cdot \mathbf{n}_j) A_j = \kappa V (I_{b,P} - I_P(\mathbf{s}_i)) \quad (4)$$

where \mathbf{n}_j is the outer unit normal vector of the surface j .

The scalar product of the i th discrete direction vector with the normal vector of the j th face of the considered cell is defined by D_{ij} as

$$D_{ij} = \mathbf{s}_i \cdot \mathbf{n}_j = \mu_i n_{xj} + \eta_i n_{yj} + \xi_i n_{zj} \quad (5)$$

The discretization of the boundary condition (Eq. (2)) is straightforward.

$$I_w = \epsilon_w I_{b,w} + \frac{1 - \epsilon_w}{\pi} \sum_{\mathbf{n} \cdot \mathbf{s}_i < 0} w_i I(\mathbf{s}_i) |\mathbf{n} \cdot \mathbf{s}_i| \quad (6)$$

For each cell, the incident radiation G is evaluated as follows:

$$G = \int_{4\pi} I(\mathbf{s}) d\Omega \approx \sum_{i=1}^{N_{dir}} w_i I(\mathbf{s}_i) \quad (7)$$

and the incident heat flux H_w at the wall surfaces is

$$H_w = \int_{\mathbf{n} \cdot \mathbf{s} < 0} I(\mathbf{s}) |\mathbf{n} \cdot \mathbf{s}| d\Omega \approx \sum_{\mathbf{n} \cdot \mathbf{s}_i < 0} w_i I_i |\mathbf{n} \cdot \mathbf{s}_i| \quad (8)$$

For a gray medium, the radiative source term S_r is given by

$$S_r = \nabla \cdot \mathbf{Q}_r = \kappa(4\pi I_b - G) \quad (9)$$

where \mathbf{Q}_r is the radiative heat flux, and the radiative net heat flux at the wall is

$$\mathbf{Q}_w = \epsilon \pi I_{b,w} - H \quad (10)$$

For the evaluation of the radiative intensity $I(\mathbf{s}_i)$ in Eqs. (6)–(10), Ströhle et al. [21] proposed a simple spatial differencing scheme based on the mean flux scheme that proved to be very efficient in the case of hybrid grids. This scheme relies on the following formulation:

$$I_P = \alpha \overline{I_{out}} + (1 - \alpha) \overline{I_{in}} \quad (11)$$

where $\overline{I_{in}}$ and $\overline{I_{out}}$ are, respectively, the intensities averaged over the entering and the exit faces of the considered cell. α is a weighting number between 0 and 1. Substituting $\overline{I_{out}}$ from Eq. (11) into Eq. (4) yields (for more details see Ref. [14])

$$I_p = \frac{\alpha V \kappa I_b - \sum_j^{D_{ij}<0} D_{ij} A_j I_j}{\alpha \kappa V + \sum_j^{D_{ij}>0} D_{ij} A_j} \quad (12)$$

The case $\alpha=1$ corresponds to the Step scheme used by Liu et al. [13]. The case $\alpha=0.5$ is called the diamond mean flux scheme (DMFS), which is formally more accurate than the step scheme. After calculation of I_p from Eq. (12), the radiation intensities at cell faces such that $D_{ij}>0$ are set equal to I_{out} , obtained from Eq. (11). For a given discrete direction, each face of each cell is placed either upstream or downstream of the considered cell center (a face parallel to the considered discrete direction plays no role). The control volumes are treated following a sweeping order such as the radiation intensities at upstream cell faces are known. This order depends on the discrete direction under consideration. An algorithm for the optimization of the sweeping order has been implemented [14]. Note that this sweeping order is stored for each discrete direction and only depends on the chosen grid and the angular quadrature, i.e., it is independent of the physical parameters or the flow and may be calculated only once, prior to the full computation.

2.1.3 Spectral Gas Properties. The absorption coefficient κ of the combustion products is highly dependent on the wave number ν , as shown by line spectra of radiative gases (H_2O , CO_2 , and CO). To take this spectral dependency into account, the absorption coefficient of each species is here represented by the *SNB-ck* model [18,22,23]. For the gas mixture composed of different species, the same model is used, building data according to the mixing model exposed by Liu et al. [23]. The radiative solutions are obtained by computing $N_{\text{bands}} \times N_{\text{quad}}$ independent calculations where $N_{\text{bands}}=367$ is the number of narrowbands of spectral width $\Delta\eta=25 \text{ cm}^{-1}$, describing the spectral properties in the range $150\text{--}9300 \text{ cm}^{-1}$, and $N_{\text{quad}}=5$ is the number of Gauss–Legendre quadrature points used for the spectral integration over each narrowband. For nongray media, introducing spectral dependencies in Eq. (9) gives for the following source term:

$$S_{r,\text{DOM}} = \sum_{i=1}^{N_{\text{band}}} \sum_{j=1}^{N_{\text{quad}}} \Delta\nu_j w_{ij} \kappa_{ij} (4\pi \bar{I}_{b,ij} - G_{ij}) \quad (13)$$

where G_{ij} is obtained from Eq. (7).

The computational efficiency of such a model is strongly linked to the number of bands N_{bands} that has to be optimized depending on the studied case.

2.2 Monte Carlo Method–Net Exchange Formulation (MCM–NEF). The code MCRAD [5,7] is based on MCM and uses computer graphics algorithms. It provides the radiative source terms and the wall heat fluxes as well as their associated statistical error estimates. One of the main features of the MCM used here is the net exchange formulation (NEF). This NEF presents some similarities with the zonal method proposed by Hottel and Sarofim [24]. This formulation that satisfies the reciprocity principle was first introduced by Green [25] in 1967. It has been applied to one-dimensional radiative heat transfer problems [6,26], to multi-dimensional problems [7,8], and very recently, to fires for benchmark solutions [5]. The NEF is the integral formulation of the radiative heat transfer, using shape factors between two volumes (Eq. (14)), a surface and a volume (Eq. (15)), or two surfaces (Eq. (16)), respectively.

$$\xi_{ij,v}^{VV} = \int_{V_j} \int_{V_i} \frac{\kappa_i \kappa_j T_{v,ij}}{s_{ij}^2} dV_i dV_j \quad (14)$$

$$\xi_{ij,v}^{VS} = \int_{S_j} \int_{V_i} \frac{\kappa_i \cdot |\mathbf{n}_i \cdot \mathbf{s}| \cdot \tau_{v,ij}}{s_{ij}^2} dV_i dS_j \quad (15)$$

$$\xi_{ij,v}^{SS} = \int_{S_j} \int_{S_i} \frac{|\mathbf{n}_i \cdot \mathbf{s}| \cdot |\mathbf{n}_j \cdot \mathbf{s}| \cdot \tau_{v,ij}}{s_{ij}^2} dS_i dS_j \quad (16)$$

with $\tau_v(s_{ij})$ the spectral transmissivity along a straight line between two points P_i and P_j expressed as

$$\tau_v(s_{ij}) = \exp \left[- \int_{s_i}^{s_j} \kappa_v(s) ds \right] \quad (17)$$

and $\Delta I_{b,v}$ the black intensity difference between these points,

$$\Delta I_{b,v} = I_{b,v}(P_i) - I_{b,v}(P_j) \quad (18)$$

These definitions allow the respective net exchange calculation:

$$\varphi_{(V_i, V_j)} = \int_0^\infty \xi_{ij,v}^{VV} \Delta I_{b,v} d\nu \quad (19)$$

$$\varphi_{(V_i, S_j)} = \int_0^\infty \xi_{ij,v}^{VS} \Delta I_{b,v} d\nu \quad (20)$$

$$\varphi_{(S_i, S_j)} = \int_0^\infty \xi_{ij,v}^{SS} \Delta I_{b,v} d\nu \quad (21)$$

where φ represents the net radiative exchange between two volumes, a volume and a surface, or two surfaces. For the sake of clarity, this formulation is presented in the case of black walls. However, the generalization of these terms to nonblack walls can be found in Ref. [8]. The radiative source term for a volume V_i or the net heat flux at a surface S_i are computed by summing their radiative exchanges with all the other volumes and surfaces.

$$\int_{V_i} S_r(\mathbf{r}_{P_i}) dV_i = \sum_{j=1}^{N_s} \varphi_{(V_i, S_j)} + \sum_{j=1}^{N_v} \varphi_{(V_i, V_j)} \quad (22)$$

and

$$q_{w,\text{net},i} = \frac{\sum_{j=1}^{N_s} \varphi_{(S_i, S_j)} + \sum_{j=1}^{N_v} \varphi_{(S_i, V_j)}}{S_i} \quad (23)$$

where N_s is the number of surfaces, and N_v is the number of volumes. The multiple integrals encountered in Eqs. (19)–(21) are calculated with a Monte Carlo method [16]. Each radiative exchange can be represented as an integral \mathbf{I} of a function g on the domain D . Defining an arbitrary probability density function p and a random variable X distributed according to p , $g(X)$ is also a random variable and \mathbf{I} is the expectation of $g(X)$. \mathbf{I} will be estimated with N samples of $g(X)$.

$$\mathbf{I} = E[g(X)] \approx \frac{1}{N} \sum_{i=1}^N g(x_i) = \langle g(X) \rangle_N$$

where x_i is a realization of X . This statistical approach provides the radiative source term and the wall heat flux with an error estimate. The standard deviation of the estimate is

$$\sigma(\langle g(X) \rangle_N) = \frac{1}{\sqrt{N}} \sigma(g(X)) \quad (24)$$

where $\sigma(g(X))$ is the standard deviation of $g(X)$ and is approximated as

$$\sigma(\mathbf{I}) \approx \frac{1}{\sqrt{N}} \sqrt{\langle (g(X))^2 \rangle_N - \langle g(X) \rangle_N^2} \quad (25)$$

Note that MCRAD uses a suitable pdf p that significantly reduces the CPU-time [6].

2.2.1 Spectral Gas Properties and k -Distribution Formulation. The spectral integrations in Eqs. (19)–(21) are carried out over narrowbands, and the k -distribution method is employed within each band. According to this method, any radiative quantity A depending on κ_ν is averaged over a band of width $\Delta\nu$ as

$$\bar{A} = \frac{1}{\Delta\nu} \int_{\Delta\nu} A(\kappa_\nu) d\nu = \int_0^\infty f(\kappa) A(\kappa) d\kappa \quad (26)$$

where $f(\kappa)$ is the distribution function of the absorption coefficient within a spectral narrowband [27]. In the case of gas mixture, the absorption coefficient at a given wave number is computed as the sum of the absorption coefficients of all gas species. For a mixture of H₂O, CO₂, and CO, one obtains

$$\bar{A} = \frac{1}{\Delta\nu} \int_{\delta\nu} A(\kappa_{\nu,\text{H}_2\text{O}} + \kappa_{\nu,\text{CO}_2} + \kappa_{\nu,\text{CO}}) d\nu \quad (27)$$

The correlated- k assumption is considered for nonhomogeneous media treatment in each narrowband, so that Eqs. (19)–(21) become

$$\begin{aligned} \varphi_{(V_i, V_j)} &= \sum_{n=1}^{n_b} \Delta\nu_n \int_0^1 dg \int_{V_i} dV_i \int_{V_j} dV_j \frac{1}{l_{ij}^2} \kappa(g) \\ &\quad \times \exp\left[-\int_{l_i}^{l_j} \kappa(g) dl\right] \kappa(g) \Delta I_{b,\nu} \\ \varphi_{(V_i, S_j)} &= \sum_{n=1}^{n_b} \Delta\nu_n \int_0^1 dg \int_{V_i} dV_i \int_{S_j} dS_j \frac{\mathbf{u} \cdot \mathbf{n}_j}{l_{ij}^2} \kappa(g) \\ &\quad \times \exp\left[-\int_{l_i}^{l_j} \kappa(g) dl\right] \Delta I_{b,\nu} \\ \varphi_{(S_i, S_j)} &= \sum_{n=1}^{n_b} \Delta\nu_n \int_0^1 dg \int_{S_i} dS_i \int_{S_j} dS_j \frac{(\mathbf{u} \cdot \mathbf{n}_i)(\mathbf{u} \cdot \mathbf{n}_j)}{l_{ij}^2} \\ &\quad \times \exp\left[-\int_{l_i}^{l_j} \kappa(g) dl\right] \Delta I_{b,\nu} \end{aligned} \quad (28)$$

where l_{ij} is the length between points i and j , \mathbf{n}_i and \mathbf{n}_j are normal vectors to surfaces at points i and j , and \mathbf{u} is the directional vector between i and j .

2.3 Accurate Solutions by MCM. In the proposed approach, the radiative solution is calculated with the DOM using either the S_4 or LC₁₁ quadrature, allowing a fast and robust computation. However the obtained solution is not exact and the error associated to each point is unknown. To evaluate the accuracy of the DOM solution, the MCM is also run at selected representative points to calculate the reference solution at these points, which play the role of probes and are chosen according to the reacting flow field topology. Finally, the analysis of the DOM results in the light of the MCM exact solutions at the probes gives a good evaluation of the full radiation field.

3 Results

3.1 Validation Test Case. The test case presented here has already been described in detail in Ref. [7] where the MCM used in MCRAD, a ray tracing method and a DOM for structured grids were compared. Here the same test case is used to compare the DOM solution on unstructured grids, performed on DOMASIUM,

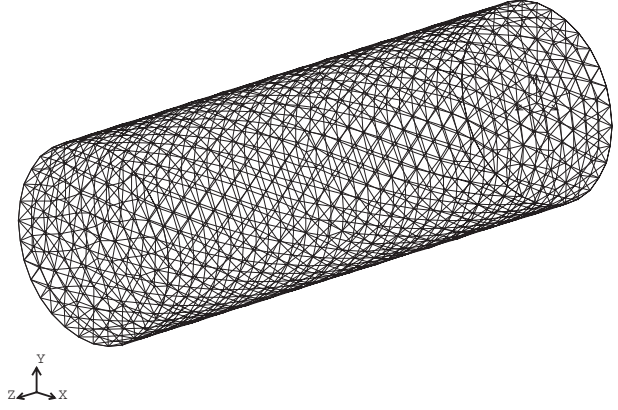


Fig. 1 Cylindrical grid (100,000 cells)

with the reference MCM solution.

The configuration is a cylindrical black walled enclosure of length L containing a mixture of water vapor, carbon dioxide, and nitrogen at atmospheric pressure. The geometrical characteristics are $L=1.2$ m and the radius is $R=0.3$ m. The wall temperature is 800 K, except at $z=L$ where it is 300 K. The temperature and concentration fields are described by the following analytical functions.

$$T(z, r) = 800 + 1200(1 - r/R)(z/L) \quad (29)$$

$$X_{\text{H}_2\text{O}}(z, r) = 0.05 \cdot [1 - 2(z/L - 0.5)^2] \cdot (2 - r/R) \quad (30)$$

$$X_{\text{CO}_2}(z, r) = 0.04 \cdot [1 - 3(z/L - 0.5)^2] \cdot (2.5 - r/R) \quad (31)$$

The DOM calculation is performed using the LC₁₁ quadrature and about 100,000 cells for the grid (Fig. 1).

The radiative source term along the central axis and the radiative heat flux at the wall are shown, respectively, in Figs. 2 and 3, where the results from both methods DOM and MCM are plotted. The associated relative errors obtained with MCM are presented in Figs. 4 and 5. Due to the fact that the unstructured grid used for the DOM calculation does not coincide with the location of the points calculated with the MCM, an interpolation procedure is needed to allow the comparison. From the MCM error estimates, the averaged relative error is found to be about 1.13% for the radiative source term and 1.98% for the radiative heat flux. Figure 3 demonstrates the high accuracy of the DOM for the wall heat

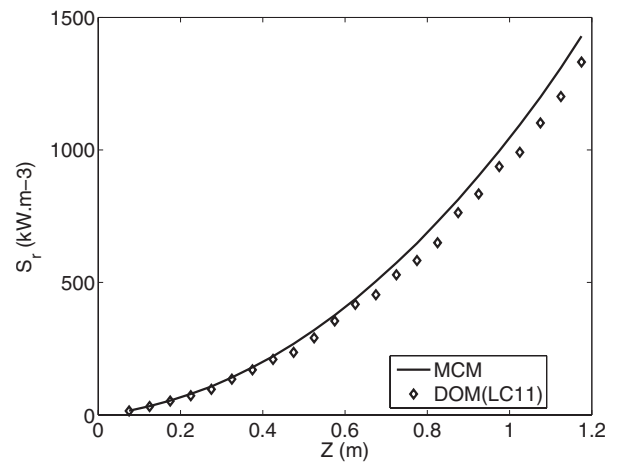


Fig. 2 Radiative source term along the central axis of the cylinder

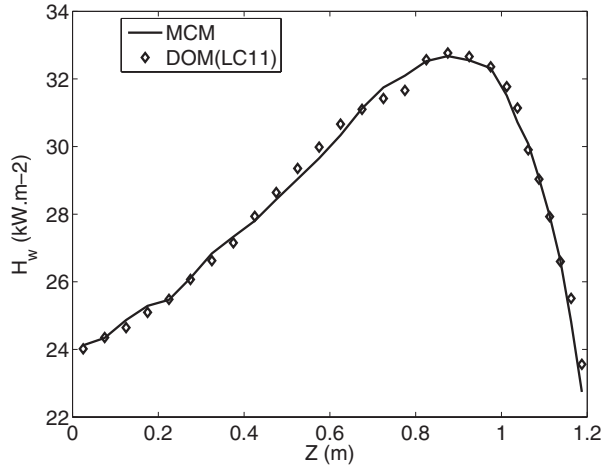


Fig. 3 Incident radiative heat flux at the wall of the cylinder

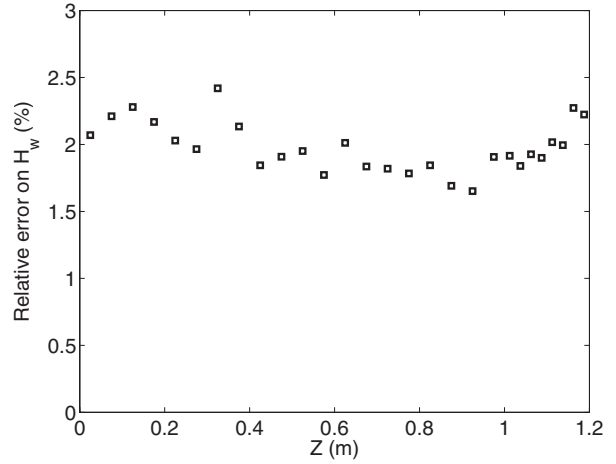


Fig. 5 Relative error associated to the MCM incident radiative heat flux at the wall of the cylinder

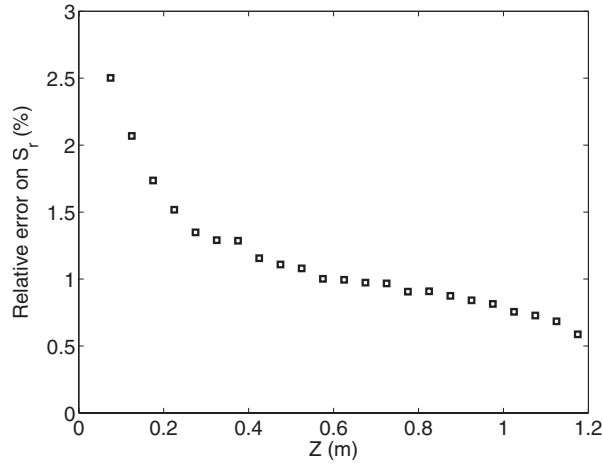


Fig. 4 Relative error associated to the MCM radiative source term along the central axis of the cylinder

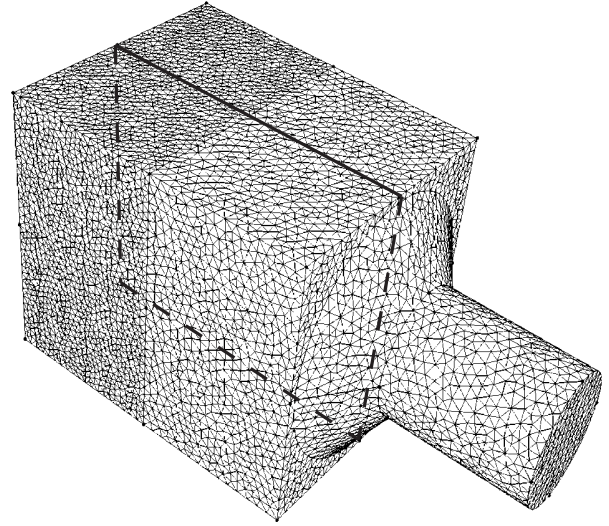


Fig. 6 Grid of the combustion chamber

flux. The source term (Fig. 2) calculated with DOM is also very accurate at the cold side of the cylinder, but a small increasing discrepancy with the MCM reference solution appears in the hot half. This discrepancy however does not exceed 10%. A first explanation may be due to the insufficient spatial discretization called “false scattering,” as explained in the parametric study of Joseph [1]. He shows that false scattering increases in DOM for increasing optical thickness. In the present case, the temperature and concentration fields (Eqs. (29) and (30)) lead to higher optical thicknesses on the hot side of the cylinder and false scattering is therefore likely to appear. Another reason for the difference between DOM and MCM may be attributed to the calculation of the species molar concentration and temperature fields themselves, which are discretized in the DOM but exactly computed from Eqs. (29) and (30) in the MCM.

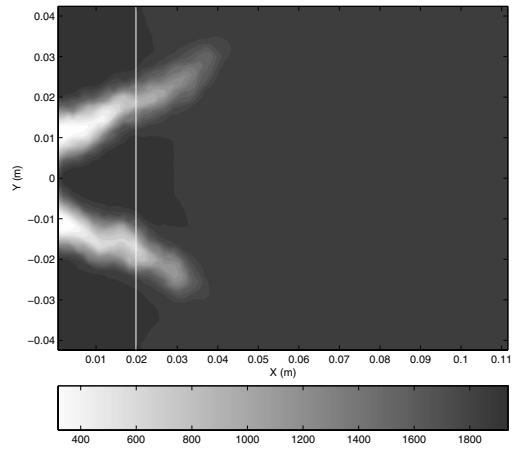
3.2 Application to a Real Combustion Chamber. This approach using the DOM method with the calibration by MCM is now performed on a complex 3D configuration of a realistic combustion chamber (Fig. 6).

Flow solutions are provided by a combustion code based on the large eddy simulation (LES) approach [28,29]: Here precomputed temperatures and concentration profiles are used to calculate the radiative source term, which means that calculation is performed

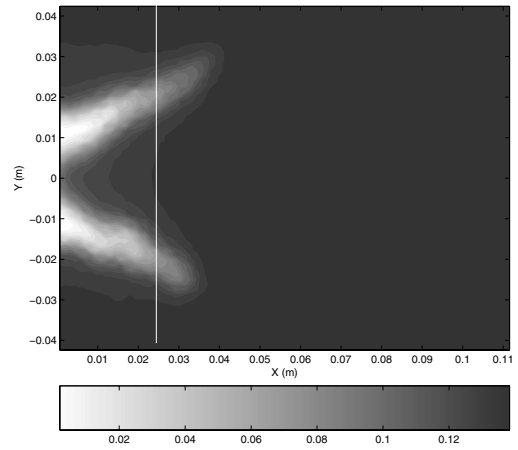
in a noncoupled way. In this test case, a swirled turbulent premixed flame is stabilized on a methane/air injection at a stoichiometric ratio of 0.75, an air flow rate of 12 g/s, and a temperature of 300 K for a thermal power of 27 kW. The chamber has a square cross section of $86 \times 86 \text{ mm}^2$ and its length is 110 mm. It ends into an exhaust duct with a 6:1 contraction. It is assumed that walls are adiabatic and may be considered as perfect radiative black bodies.

The flame/turbulence interaction is modeled by the thickened flame/efficiency function model [30,31] and the chemical scheme for combustion takes into account two reactions with six species (CH_4 , O_2 , CO_2 , CO , H_2O , and N_2) [32]. The molar concentrations of CO_2 , CO , H_2O , O_2 , and N_2 are used to determine the radiative spectral properties of the mixture. Figure 7 shows a 2D view in the cutting median plane defined on Fig. 6 of the temperature and radiative species molar fractions fields obtained from the LES and used for the radiation calculation. The corresponding heat release $\dot{\omega}$ is shown on Fig. 8.

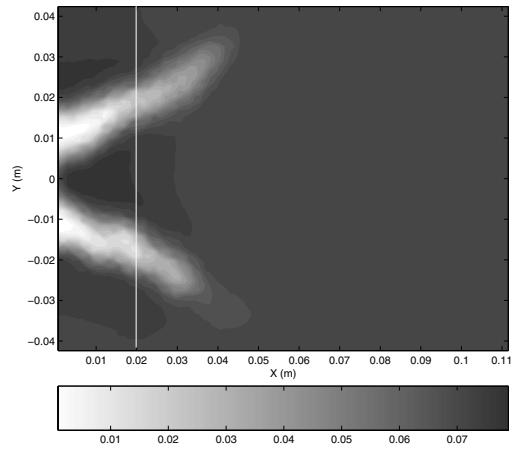
The flame has the classical conical shape found in this type of burners. It is attached to the injector and deviated from the central axis by the swirling flow that creates a central recirculation zone. The maximum heat release is of the order of $7 \times 10^8 \text{ J m}^{-3} \text{ s}^{-1}$,



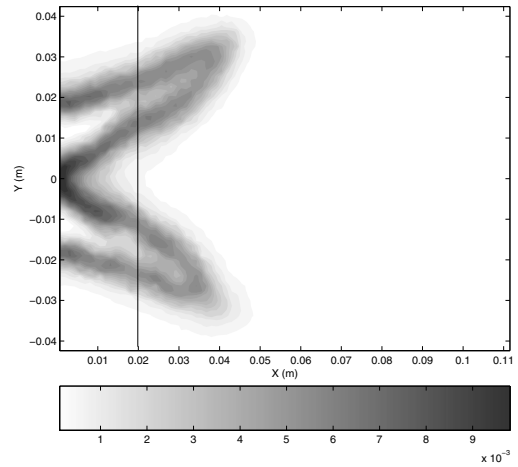
(a) The temperature



(b) X_{H_2O} profile



(c) X_{CO_2} profile



(d) X_{CO} profile

Fig. 7 Instantaneous solution fields in the median cutting plane of the combustion chamber: temperature and radiative species concentration; (a) temperature profile, (b) X_{H_2O} profile, (c) X_{CO_2} profile, and (d) X_{CO} profile

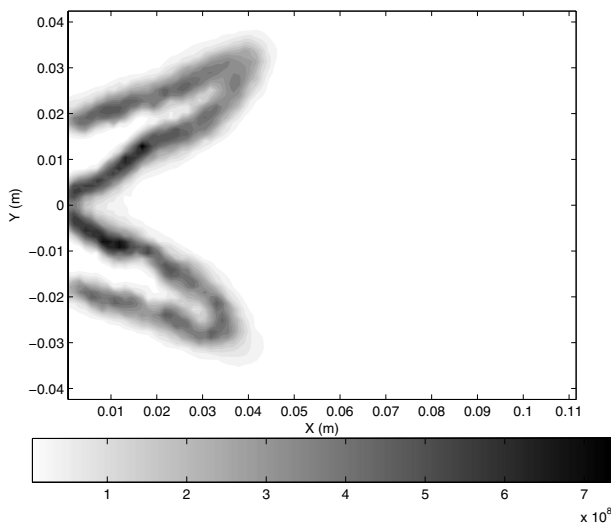


Fig. 8 Instantaneous heat release $\dot{\omega}$ in the median cutting plane of the combustion chamber

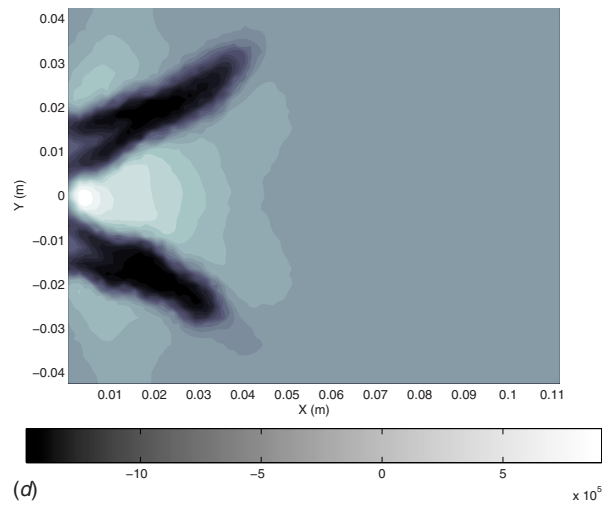


Fig. 9 Instantaneous radiative source term in the median cutting plane of the combustion chamber; calculation with DOM- S_4 quadrature

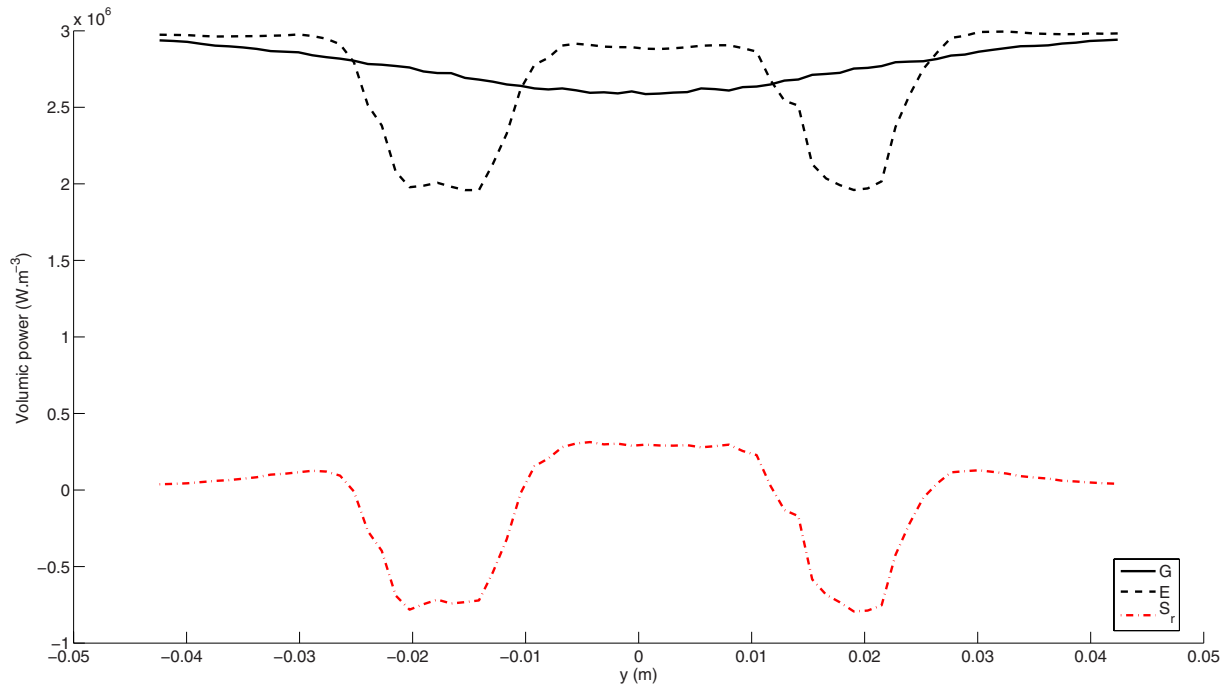


Fig. 10 Radiative incident heat flux G , radiative emitted heat flux E , and radiative source term S_r along the y -axis located at $x=0.02$ m in the median plane of the combustion chamber; calculation with DOM-LC₁₁ quadrature

leading to a maximum temperature of about 1900 K.

Figure 9 represents the corresponding instantaneous radiative source term obtained from DOM with the S_4 quadrature. The maximum value is of the order of $10^6 \text{ J m}^{-3} \text{ s}^{-1}$, i.e., two orders of magnitude smaller than the maximum heat release.

However it is interesting to note that the location of the maxima of these two energy source terms is completely different: the heat

release is maximum at the flame front location, i.e., at the frontier between cold and hot gases, whereas the absolute value of the radiative source term is highest in the cold gas region, where there is strong absorption. This is due to the presence of absorbing chemical species (combustion products that have diffused in the unburnt gas) in these regions at a low temperature. This may give locally a significant contribution to the total gas energy, and fi-

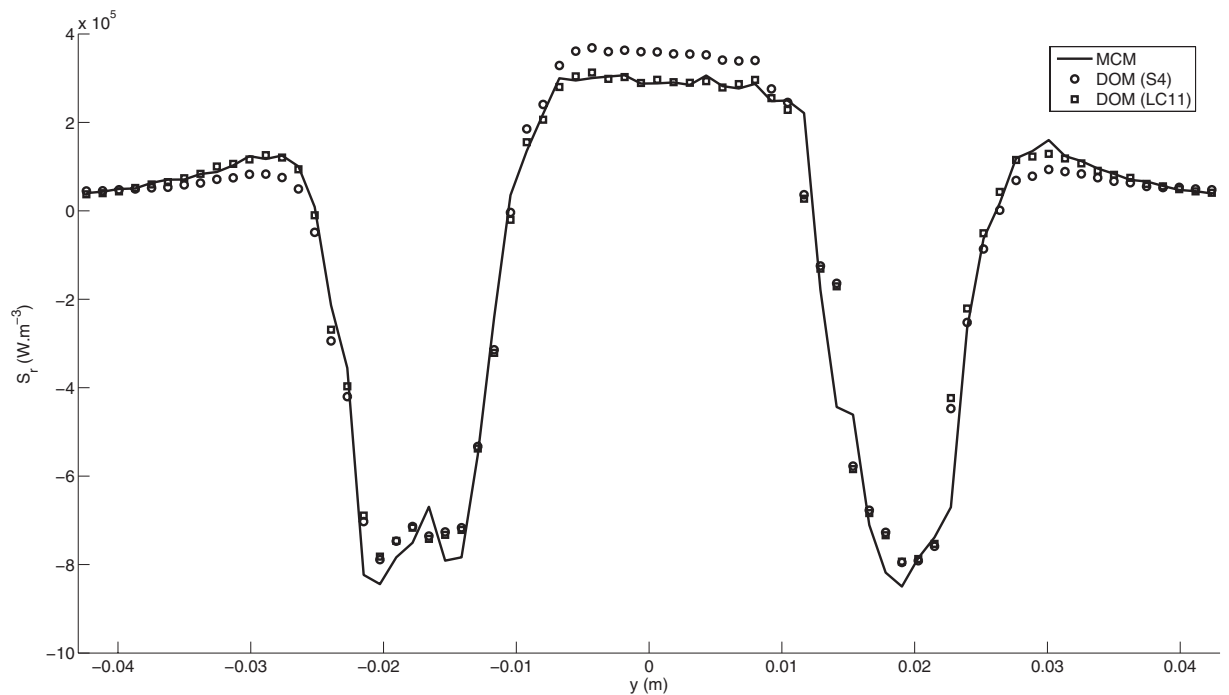


Fig. 11 Radiative source term along the y -axis located at $x=0.02$ m in the median plane of the combustion chamber; calculation with DOM- S_4 quadrature, DOM-LC₁₁ quadrature, and MCM

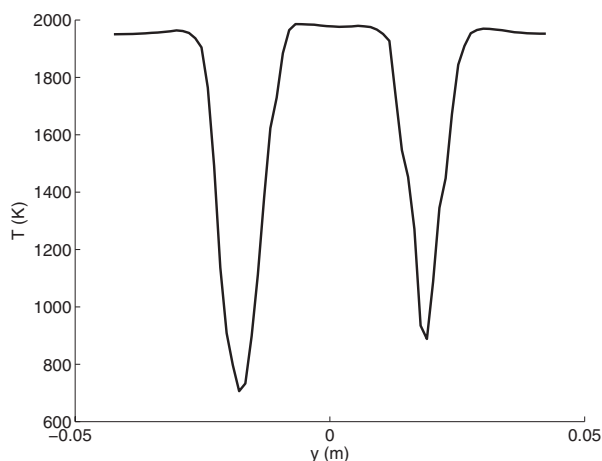


Fig. 12 Temperature profile along the y -axis located at $x=0.02$ m in the median plane of the combustion chamber

nally lead to a potential high impact on the flame structure and the flow. Figure 10 represents the emitted part E and the incident part G of the radiative heat fluxes that sum to the radiative source term S_r . It appears that the radiative exchanges E and G are of the same order of magnitude and that both are higher than the source term.

Therefore in this case, a simple model based on emission only (as the optically thin model) would clearly lead to a wrong source term, which is expected to have a strong impact on minor species prediction.

The same calculation was also performed with the LC_{11} quadrature and a comparison is shown on Fig. 11, where the radiative source term (Fig. 9) is plotted along a line at $x=0.02$ m for the two DOMs (S_4 and LC_{11}) and the MCM calculations. The corresponding temperature and radiative species molar fractions profiles are represented along the same axis in Figs. 12 and 13. The averaged relative error on the MCM solution is found to be 3.17%.

The flame impact is well represented by the three methods. The solution modeled with the LC_{11} (96 discrete directions) is in excellent agreement with the reference solution, with a maximum error of 3%, confirming the already known high accuracy of this method. As expected the S_4 quadrature calculation is less accurate, in particular, in the vicinity of the flame fronts. Note that the radiative source term is either underestimated (outside the conical

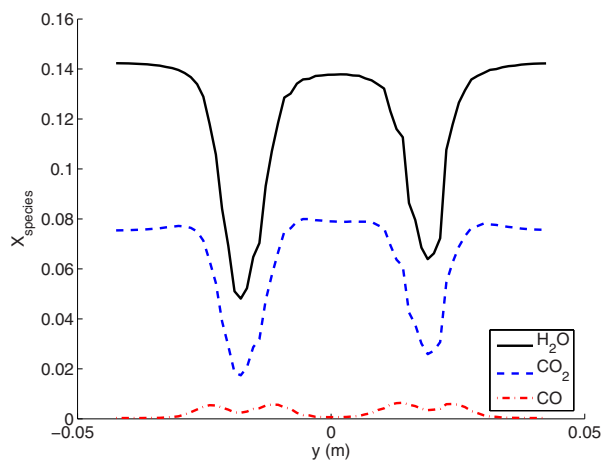


Fig. 13 Radiative species molar fractions profiles along the y -axis located at $x=0.02$ m in the median plane of the combustion chamber

flame) or overestimated (inside the conic flame), although the temperature and species concentrations, and as a consequence, the emission E are nearly constant in these zones (Figs. 12, 13, and 10).

The underestimation and the overestimation of the radiative source term S_r obtained with the S_4 quadrature are located in zones where the temperature and radiative species concentrations are maximum. This is an indication for the source error, probably due to a lack of angular resolution, and illustrates clearly the benefit of using the DOM with MCM error control. Without the reference solution, it would be impossible to identify and estimate such an error. Still the maximum error does not exceed 20% in very localized zones, and one may conclude that for most combustion applications, the accuracy of the DOM with the S_4 (24 discrete directions) quadrature is sufficient.

In the perspective of coupling radiation calculations with unsteady combustion simulations, the advantages of the DOM with MCM error control approach appear also clearly in the light of CPU cost. While for the present case, the DOM takes 4 ms/cell for each discrete direction, the MCM calculation time is of the order of a few seconds per point on the same computer.

4 Conclusions

The full coupling of radiation with unsteady combustion is a key point in the development of predictive simulation tools for industrial burners. It requires fast and accurate radiative models, in accordance with the needs of the combustion models. In this context, a DOM with MCM error control is proposed, which cumulates the advantages of both classes of methods. The validity and potential of this methodology is demonstrated on both academic and complex industrial test cases. It is shown how the effective accuracy of an approximate DOM solution is estimated with the MCM, leading to an optimal choice of parameters of the DOM and the best compromise between accuracy and efficiency.

The next step toward radiation-combustion coupled simulations is the improvement of computational resources management and an automatic control procedure using MCM probe solutions. Simpler and faster spectral radiative property models will also reduce the radiation computing time without a significant loss of accuracy, down to a time of the same order of magnitude than the combustion simulations. These developments are currently in progress and first attempts of coupled simulations have already been successful [33–36].

Acknowledgment

The support of Turbomeca and the EC project PRECCINSTA (EU Contract No. ENK5-CT-2000-00060) is gratefully acknowledged for providing the CFD data.

Special thanks to Professor Fournier of the University Paul Sabatier for his guidance and fruitful discussions.

References

- [1] Joseph, D., 2004, "Modélisation des transferts radiatifs en combustion par méthode aux ordonnées discrètes sur des maillages non structurés tridimensionnels," Institut National Polytechnique de Toulouse.
- [2] Beltrame, A., Porshnev, P., Merchan-Merchan, W., Savelier, A., Kennedy, L. A., Petrova, O., Zhdanok, S., Amouri, F., and Charon, O., 2001, "Soot and NO Formation in Methane-Oxygen Enriched Diffusion Flames," *Combust. Flame*, **124**, pp. 295–310.
- [3] Hall, R. J., Smooke, M. D., and Colket, M. B., 1997, "Predictions of Soot Dynamics in Opposite Jets Diffusion Flames," *Physical and Chemical Aspects of Combustion: A Tribute to Irvin Glassman*, Academic, New York.
- [4] Mbiok, M., and Weber, R., 2000, *Radiation in Enclosures*, Springer-Verlag, Berlin.
- [5] Jensen, K. A., Ripoll, J. F., Wray, A. A., Joseph, D., and El Hafi, M., 2007, "On Various Modeling Approaches for Radiative Heat Transfer in Pool Fires," *Combust. Flame*, **148**(4), pp. 263–279.
- [6] de Lataillade, A., Dufresne, J. L., El Hafi, M., Eymet, V., and Fournier, R., 2002, "A Net Exchange Monte Carlo Approach to Radiation in Optically Thick Systems," *J. Quant. Spectrosc. Radiat. Transf.*, **74**(5), pp. 563–584.
- [7] Coelho, P. J., Perez, P., and El Hafi, M., 2003, "Benchmark Numerical Solutions for Radiative Heat Transfer in Two-Dimensional Axisymmetric Enclo-

- tures With Nongray Sooting Media," *Numer. Heat Transfer, Part B*, **43**, pp. 425–444.
- [8] Perez, P., El Hafi, M., Coelho, P. J., and Fournier, R., 2005, "Accurate Solutions for Radiative Heat Transfer in Two-Dimensional Axisymmetric Enclosures With Gas Radiation and Reflective Surfaces," *Numer. Heat Transfer, Part B*, **47**, pp. 39–63.
- [9] Tessé, L., Dupoirieux, F., and Taine, J., 2004, "Monte Carlo Modeling of Radiative Transfer in a Turbulent Sooty Flame," *Int. J. Heat Mass Transfer*, **47**, pp. 555–572.
- [10] De Lataillade, A., Blanco, S., Clergent, Y., Dufresne, J. L., El Hafi, M., and Fournier, R., 2002, "Monte Carlo Methods and Sensitivity Estimations," *J. Quant. Spectrosc. Radiat. Transf.*, **75**, pp. 529–538.
- [11] Roger, M., Blanco, S., El Hafi, M., and Fournier, R., 2005, "Monte Carlo Estimates of Domain Deformation Sensitivities," *Phys. Rev. Lett.*, **95**, p. 180601.
- [12] Modest, M. F., 2003, *Radiative Heat Transfer*, 3rd ed., McGraw-Hill, New York.
- [13] Liu, J., Shang, H. M., Chen, Y. S., and Wang, T. S., 2000, "Development of an Unstructured Radiation Model Applicable for Two Dimensional Planar, Axisymmetric and 3-Dimensional Geometries," *J. Quant. Spectrosc. Radiat. Transf.*, **66**, pp. 17–33.
- [14] Joseph, D., El Hafi, M., Fournier, R., and Cuenot, B., 2005, "Comparison of Three Spatial Differencing Schemes in Discrete Ordinates Method Using Three-Dimensional Unstructured Meshes," *Int. J. Therm. Sci.*, **44**(9), pp. 851–864.
- [15] Lockwood, F. C., and Shah, N. G., 1981, "A New Radiation Solution Method for Incorporation in General Combustion Prediction Procedures," 18th Symposium (International) on Combustion, The Combustion Institute, pp. 1405–1409.
- [16] Perez, P., 2003, "Algorithmes de synthèse d'images et propriétés spectrales des gaz de combustion: méthode de Monte Carlo pour la simulation des transferts radiatifs dans les procédés à haute température," Institut National Polytechnique de Toulouse.
- [17] Liu F., 1999, "Numerical Solutions of Three-Dimensional Non-Grey Gas Radiative Transfer Using the Statistical Narrow-Band Model," *ASME J. Heat Transfer*, **121**, pp. 200–203.
- [18] Soufiani, A., and Taine, J., 1997, "High Temperature Gas Radiative Property Parameters of Statistical Narrow Band Model for H₂O, CO₂ and CO and Correlated-K Model for H₂O and CO₂," *Int. J. Heat Mass Transfer*, **40**(4), pp. 987–991.
- [19] Chandrasekhar, S., 1950, *Radiative Transfer*, Clarendon, Oxford.
- [20] Koch, R., and Becker, R., 2003, "Evaluation of the Quadrature Schemes for the Discrete Ordinates Method," *Proceedings of Eurotherm73 on Computational Thermal Radiation in Participating Media*, Eurotherm Series No. 11, P. Lybaert, V. Feldheim, D. Lemonnier, and N. Selçuk, eds., Elsevier, Paris, pp. 59–74.
- [21] Ströhle, J., Schnell, U., and Hein, K. R. G., 2001, "A Mean Flux Discrete Ordinates Interpolation Scheme for General Coordinates," Third International Conference on Heat Transfer, Antalya.
- [22] Liu, F., Smallwood, G. J., and Gülder, Ö. L., 2000, "Application of the Statistical Narrow-Band Correlated-*k* Method to Low-Resolution Spectral Intensity and Radiative Heat Transfer Calculations—Effects of the Quadrature Scheme," *Int. J. Heat Mass Transfer*, **43**, pp. 3119–3135.
- [23] Liu, F., Smallwood, G. J., and Gülder, Ö. L., 2001, "Application of the Statistical Narrow-Band Correlated-*k* Method to Non-Grey Gas Radiation in CO₂–H₂O Mixtures: Approximate Treatments of Overlapping Bands," *J. Quant. Spectrosc. Radiat. Transf.*, **68**, pp. 401–417.
- [24] Hottel, H. C., and Sarofim, A. F., 1967, *Radiative Transfer*, McGraw-Hill, New York.
- [25] Green, J. S. A., 1967, "Division of Radiative Streams Into Internal Transfer and Cooling to Space," *Q. J. R. Meteorol. Soc.*, **93**, pp. 371–372.
- [26] Cherkaoui, M., Dufresne, J. L., Fournier, R., Grandpeix, J. Y., and Lahellec, A., 1996, "Monte Carlo Simulation of Radiation in Gases With a Narrow-Band Model and a Net-Exchange Formulation," *ASME J. Heat Transfer*, **118**, pp. 401–407.
- [27] Dufresne, J.-L., Fournier, R., and Grandpeix, J.-Y., 1999, "Inverse Gaussian *K*-Distributions," *J. Quant. Spectrosc. Radiat. Transf.*, **61**, pp. 433–441.
- [28] Schönfeld, T., and Rudgyard, M., 1999, "Steady and Unsteady Flows Simulations Using the Hybrid Flow Solver AVBP," *AIAA J.*, **37**(11), pp. 1378–1385.
- [29] Roux, S., Lartigue, G., Poinso, T., Meier, U., and Bérat, C., 2005, "Studies of Mean and Unsteady Flow in a Swirled Combustor Using Experiments, Acoustic Analysis and Large Eddy Simulations," *Combust. Flame*, **141**, pp. 40–54.
- [30] Angelberger, C., Egolfopoulos, F., and Veynante, D., 2000, "Large Eddy Simulations of Chemical and Acoustic Forcing of a Premixed Dump Combustor," *Flow, Turbul. Combust.*, **65**(2), pp. 205–222.
- [31] Colin, O., Ducros, F., Veynante, D., and Poinso, T., 2000, "A Thickened Flame Model for Large Eddy Simulations of Turbulent Premixed Combustion," *Phys. Fluids*, **12**(7), pp. 1843–1863.
- [32] Selle, L., Lartigue, G., Poinso, T., Koch, R., Schildmacher, K. U., Krebs, W., Prade, B., Kaufmann, P., and Veynante, D., 2004, "Compressible Large Eddy Simulations of Turbulent Combustion on Complex Geometries on Unstructured Meshes," *Combust. Flame*, **137**, pp. 489–505.
- [33] Goncalves dos Santos, R., Lecanu, M., Ducruix, S., Gicquel, O., and Veynante, D., 2005, "Large Eddy Simulations of Combustion/Radiative Heat Transfers Coupling Using the Specialized Communication Language CORBA," The Cyprus International Symposium on Complex Effects in Large Eddy Simulations, Limassol, Cyprus, Sept. 20–25.
- [34] Goncalves dos Santos, R., Ducruix, S., Gicquel, O., and Veynante, D., 2006, "Large Eddy Simulations of Turbulent Combustion Including Radiative Heat Transfers Using Specialised Communication Languages," 11th International Conference on Numerical Combustion, Granada, Spain.
- [35] Goncalves dos Santos, R., Ducruix, S., Gicquel, O., Joseph, D., El Hafi, M., and Veynante, D., 2007, "Large-Eddy Simulations Including Radiative Heat Transfer," Third European Combustion Meeting, Chania, Crete, Apr. 11–13, Paper No. 23–3.
- [36] Goncalves dos Santos, R., Lecanu, M., Ducruix, S., Gicquel, O., Iacona, E., and Veynante, D., 2008, "Coupled Large Eddy Simulations of Turbulent Combustion and Radiative Heat Transfer," *Combust. Flame*, **152**(3), pp. 387–400.